Intrinsically disordered protein biosensor tracks the physical-chemical effects of osmotic stress on cells

Cesar L Cuevas-Velazquez[1,2,3,4*], Tamara Vellosillo[1,2], Karina Guadalupe[5,6], H Broder Schmidt[7], Feng Yu[5,8], David Moses[5,6], Jennifer AN Brophy[1,2], Dante Cosio-Acosta[3], Alakananda Das[9], Lingxin Wang[9], Alexander M Jones[10], Alejandra A Covarrubias[3*], Shahar Sukenik[5,6,8*], José R Dinneny[1,2,11*]

[1] Department of Biology, Stanford University, Stanford, CA, 94305, USA
[2] Department of Plant Biology, Carnegie Institution for Science, Stanford, CA, 94305, USA
[3] Departamento de Biología Molecular de Plantas, Instituto de Biotecnología, Universidad Nacional Autónoma de México, Cuernavaca, Mor., 62210 Mexico
[4] Departamento de Bioquímica, Facultad de Química, Universidad Nacional Autónoma de México, Ciudad de México, 04510, Mexico
[5] Center for Cellular and Biomolecular Machines (CCBM), University of California, Merced, CA, 95343, USA
[6] Chemistry and Chemical Biology Program, University of California, Merced, CA, 95343, USA
[7] Department of Biochemistry, Stanford University School of Medicine, Stanford, CA, 94305, USA
[8] Quantitative Systems Biology Program, University of California, Merced, CA, 95343, USA
[9] Department of Molecular and Cellular Physiology, Stanford University, Stanford, CA, 94305, USA
[10] Sainsbury Laboratory, Cambridge University, Cambridge, CB2 1LR, UK
[11] Lead Contact
* Correspondence C.L.C.V. cuevas@quimica.unam.mx
* Correspondence A.C.R. alejandra.covarrubias@mail.ibt.unam.mx
* Correspondence S.S. ssukenik@ucmerced.edu
* Correspondence J.R.D. dinneny@stanford.edu

SUMMARY

Cell homeostasis is perturbed when dramatic shifts in the external environment cause the physical-chemical properties inside the cell to change. Methods that dynamically monitor these intracellular effects are currently lacking. Here, we leveraged the environmental sensitivity and structural plasticity of intrinsically disordered regions (IDRs) to develop a FRET biosensor capable of monitoring rapid intracellular changes caused by osmotic stress. The biosensor, named SED1, utilizes the Arabidopsis intrinsically disordered AtLEA4-5 protein expressed in plants under water deficit. Computational modeling and *in vitro* studies reveal that SED1 is highly sensitive to macromolecular crowding. SED1 exhibits large and near-linear osmolarity-dependent changes in FRET inside living bacteria, yeast, plant, and human cells, demonstrating the broad utility of this tool for studying water-associated stress. This study demonstrates the remarkable ability of IDRs to sense the cellular environment across the tree of life and provides a blueprint for their use in environmentally-responsive molecular tools.

INTRODUCTION

Intracellular osmotic fluctuations are one of the most common physicochemical perturbations cells experience throughout their life (Li et al., 2020). In the absence of external stressors, the metabolic activity of the cell can induce large changes in the concentration of different metabolites that alter intracellular osmolarity (Yancey, 2005). Additional osmotic variations can be caused by the activity of ion channels that change the total concentration of free inorganic ions (K^+, Na^+, Mg^{2+}, etc.) (Hosseiniyan Khatibi et al., 2019). Severe intracellular osmotic perturbations are readily caused by environmentally-induced stress conditions, where the osmolarity outside of the cells changes dramatically. For instance, a decrease in water content in the exterior of a cell increases extracellular osmolarity in a way that causes the passive efflux of water out of the cell. This results in an immediate collapse of cell volume and concomitant increase in the concentration of solutes, macromolecular crowding, and the viscosity of the cell interior, impacting a plethora of molecular and cellular functions (Persson et al., 2020; Record et al., 1998; Spitzer and Poolman, 2009; Sukenik et al., 2017).

Despite the importance of osmotic regulation on cell function, our mechanistic understanding of how cells sense such conditions, particularly in multicellular organisms, is limited (Bourque, 2008; Haswell and Verslues, 2015). One of the main barriers to better understanding the intracellular effects of osmotic stress is the lack of methods to reliably monitor physical-chemical changes that occur in single cells, in real time, and in a non-destructive manner (Haswell and Verslues, 2015; Nongpiur et al., 2020; Scharwies and Dinneny, 2019).

Genetically encoded fluorescent biosensors are optical tools that enable the dynamic visualization and quantification of biochemical events that occur in living cells at various scales, from single cells to whole organisms (Zhou et al., 2020). Fluorescent biosensors are chimeric proteins composed of at least one fluorescent protein fused to a sensing domain. The selection of the sensing domain is based

on its ability to specifically change its conformation in the presence or absence of an analyte (Okumoto et al., 2012). The conformational change of the sensing domain then causes a change in the fluorescence readout that can be quantified. As of today, there are dozens of different fluorescent biosensors used to track small molecules, phosphorylation events, neurotransmitters, posttranslational modifications, and hormones; however, just a small fraction of biosensors are designed to report changes in the physical-chemical properties of the environment (Boersma et al., 2015; Greenwald et al., 2018; Liu et al., 2017; Mahon, 2011; Pittas et al., 2020). The main challenge for developing environmentally-responsive biosensors is in sourcing sensory domains capable of specifically and reversibly altering their structure in response to changes in a specific physical-chemical property.

Intrinsically disordered regions (IDRs) are protein domains that lack a stable tertiary structure and instead behave as ensembles of dynamic and rapidly changing conformations (Wright and Dyson, 2015). Because IDRs have a more extended surface area than globular proteins, they are highly sensitive to the physical-chemical properties of the solvent. Conditions such as pH, temperature, redox state, and high osmolarity induce conformational changes in some IDRs (Theillet et al., 2014). Recent work shows that environmental sensitivity is a shared property of many IDRs (Holehouse and Sukenik, 2020; Moses et al., 2020). Furthermore, it has been proposed that the environmental sensitivity of IDRs could be used to regulate their activity, potentially allowing them to function as sensors of the environment (Cuevas-Velazquez and Dinneny, 2018; Scharwies and Dinneny, 2019; Yoo et al., 2019). Based on the aforementioned properties, we propose that IDRs are promising candidates for use in the development of environmentally-responsive biosensors.

Here, we report the design, development and implementation of a Förster Resonance Energy Transfer (FRET) biosensor that tracks the effects of osmotic stress on living cells from a wide variety of organisms. For the sensory domain we tested a group of hyperosmotic-induced IDRs from plants. Specifically, we used group 4 LATE EMBRYOGENESIS ABUNDANT (LEA) proteins from the model plant *Arabidopsis thaliana* (Olvera-Carrillo et al., 2010), which we previously reported are intrinsically disordered proteins that exhibit conformational rearrangements *in vitro* upon changes in the osmolarity of the solution (Cuevas-Velazquez et al., 2016). Initial screening of prototype biosensors in budding yeast revealed that these proteins, particularly AtLEA4-5, undergo a rapid and reversible conformational change in response to hyperosmotic treatments with different osmolytes in cells. All-atom simulations and *in vitro* experiments revealed that the physical dimensions of the AtLEA4-5 conformational ensemble can change dramatically when the composition of the surrounding solution is altered, supporting our findings in living cells. The resulting FRET biosensor, named SENSOR EXPRESSING DISORDERED PROTEIN 1 (SED1), can dynamically monitor the response of budding yeast to osmotic stress at the cellular level. SED1 can also be used to track the effects of osmotic stress on live bacteria (*Escherichia coli*) cells, plant (*Nicotiana benthamiana*) cells, and U-2 OS human cells. The use of fluorescent biosensors such as SED1 will aid in understanding how cells sense, respond, and acclimate to dynamic environmental fluctuations caused by water-associated stress.

RESULTS

Design of a biosensor for studying the effects of osmotic stress on living cells

To track the effects of osmotic stress on living cells, we sought to combine the power of osmo-sensitive IDRs and ratiometric FRET readouts to build a genetically encoded fluorescent biosensor. For the sensory domain, we tested two members of the group 4 LEA proteins from the model plant *Arabidopsis thaliana* (Olvera-Carrillo et al., 2010). Group 4 LEA proteins are IDPs that exhibit a reversible disorder-to-folded transition in response to increased osmolarity *in vitro* (Cuevas-Velazquez et al., 2016). We hypothesized that such osmolarity-dependent conformational changes would also occur inside living cells, making them excellent candidates for environmentally-responsive biosensor development.

To test the ability of group 4 LEA protein structure to change in response to osmotic stress *in vivo*, we fused either *AtLEA4-2* or *AtLEA4-5* ORFs between the coding sequences of a FRET-compatible pair of fluorophores (mCerulean3 as the donor and mCitrine as the acceptor) (Figure 1A). These constructs were expressed in live budding yeast (*Saccharomyces cerevisiae*) cells and treated with NaCl to induce hyperosmotic shock. Both constructs exhibited a NaCl-concentration-dependent increase in the acceptor-to-donor emission ratio (Figure 1B). We observed that the treatment displayed typical FRET behavior with an increase in fluorescence intensity of the acceptor (donor excitation-acceptor emission; DxAm) coupled to a decrease in fluorescence intensity of the donor (donor excitation-donor emission; DxDm) (Figure 1C and Figure S1A), leading to a higher acceptor to donor emission ratio (DxAm/DxDm) (Figure 1B). The FRET ratio change was significantly smaller when we tested a globular protein (arabinose-binding protein, ABP) as a reference (Kaper et al., 2008) (Figure 1B and Figure S1B). Hyperosmotic treatment with increasing concentrations of other ionic (Figure S1C) and non-ionic (Figure S1D) osmolytes showed that the change in FRET of both constructs is osmolarity-dependent and not osmolyte-specific (Figures S1E and S1F). Since AtLEA4-5 exhibited the largest FRET change in response to osmotic shock, we continued our characterization with this construct. The fluorescence intensity of single mCerulean3 or mCitrine fused to AtLEA4-5 was not significantly affected by hyperosmotic shock induced with different solutes, demonstrating the stability of the

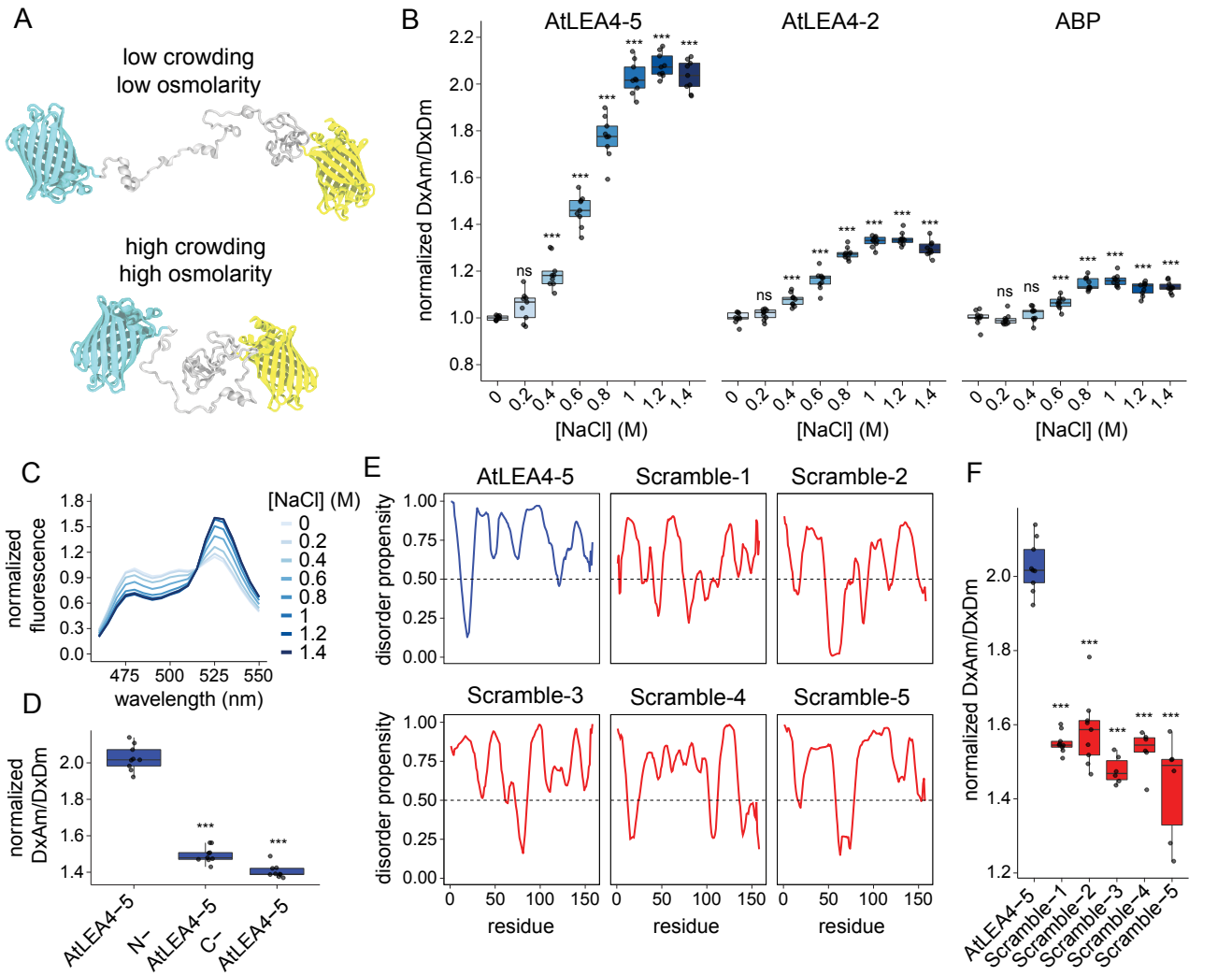

Figure 1. Design of a biosensor for studying the effects of osmotic stress on living cells. (A) Schematic representation of the biosensor design under low and high macromolecular crowding/osmolarity - prevalent intracellular conditions upon hypoosmotic or hyperosmotic stress, respectively. The conformations are selected from the ensemble of all-atom simulations of AtLEA4-5 in the corresponding conditions. Cyan: mCerulean3. Yellow: mCitrine. Gray: AtLEA4-5. (B) Normalized FRET ratio (DxAm/DxDm) of live yeast cells treated with different concentrations of NaCl. Cells are expressing the biosensor construct using either AtLEA4-5, AtLEA4-2, or arabinose binding protein (ABP) as the sensory domain. Two-way ANOVA. *p < 0.05, **p < 0.01, ***p < 0.001. (C) Fluorescence emission spectra of NaCl-treated live yeast cells expressing the biosensor construct using AtLEA4-5 as the sensory domain. Fluorescence values were normalized to the value at 515 nm. (D) Normalized FRET ratio (DxAm/DxDm) of live yeast cells expressing either AtLEA4-5, N-AtLEA4-5, or C-AtLEA4-5 biosensor constructs. Cells were treated with 1 M NaCl. One-way ANOVA. *p < 0.05, **p < 0.01, ***p < 0.001. (E) Disorder propensity prediction of AtLEA4-5 (blue) and five different scrambled versions (red) using PONDR. Threshold at 0.5 disorder propensity is shown. (F) Normalized FRET ratio (DxAm/DxDm) of live yeast cells expressing AtLEA4-5 (blue) or five different scrambled versions (red). One-way ANOVA. *p < 0.05, **p < 0.01, ***p < 0.001.

fluorophores in such conditions (Figures S1G and S1H). Finally, testing ten different FRET pairs revealed that the mCerulean3-mCitrine pair had the highest dynamic range among monomeric fluorescent proteins (Figure S2).

We searched for the sequence determinants of AtLEA4-5 environmental responsiveness. To do so, we split the full sequence into its two functional domains (termed N-terminal conserved domain and C-terminal variable domain, based on their sequence similarity to other LEA proteins), individually introduced them into the FRET system, and expressed them in live yeast cells. The N-terminal conserved domain has the ability to fold into an α-helix upon increased osmolarity *in vitro*, while the C-terminal variable domain remains largely disordered (Cuevas-Velazquez et al., 2016), suggesting that deletion of the latter may enhance the osmo-sensitivity of our reporter. However, we found that full-length AtLEA4-5 is necessary to reach the highest FRET ratio change upon hyperosmotic treatment (Figure 1D), suggesting that both domains are required for the full conformational change *in vivo*.

Next, we tested how primary amino acid sequence and composition of AtLEA4-5 affected the dynamic FRET

properties of our reporter. We synthesized five different scrambled versions of the AtLEA4-5 coding sequence holding the amino acid composition constant (Figure S3A). We designed the scrambled versions to remain highly disordered, but with a decreased propensity, relative to AtLEA4-5, to form an α-helix (Figure 1E and Figure S3B). When these sequences were used to generate FRET reporters and expressed in yeast, we found that the different scrambled versions displayed a diminished magnitude of FRET response to hyperosmotic stress compared to the native AtLEA4-5 sequence (Figure 1F). Together these results suggest that the AtLEA4-5 protein is able to undergo osmotic-stress-induced conformational changes *in vivo*, and that these changes are dependent on the full-length primary amino acid sequence of the protein.

AtLEA4-5 is highly sensitive to the chemical composition of the solution

As water leaves the cell during hyperosmotic shock, a number of physical-chemical properties of the intracellular environment change; in particular, the concentration of organic and inorganic solutes rises, as does the extent of macromolecular crowding. Any of these properties could underlie the biophysical mechanism driving the conformational changes in AtLEA4-5. Macromolecular crowding is a general condition of the cell interior that gets exacerbated under hyperosmotic conditions due to water loss (Heo et al., 2008; Jalihal et al., 2020; Mika and Poolman, 2011). In order to further investigate the mechanism of AtLEA4-5 responsiveness observed in cells, we designed an approach to test AtLEA4-5 sensitivity to different solutions *in silico* and *in vitro*.

First, we performed all-atom Monte Carlo simulations to sample the conformational landscape of AtLEA4-5 under a wide range of solution conditions. This class of simulation, known as solution space (SolSpace) scanning, has been used to investigate the solution-protein interactions of dozens of IDRs (Holehouse and Sukenik, 2020; Moses et al., 2020). We used this method to exert a compacting force on a range of IDRs and compared the tendency of the different sequences to compact. We observed that AtLEA4-5 shows an enhanced sensitivity to such compaction compared to the scrambled versions of the sequence, in agreement with our *in vivo* observations (Figure 2A and Figure 1F). Furthermore, a comparison with 70 different naturally occurring IDRs shows that AtLEA4-5 is an outlier in terms of its sensitivity (Figure 2A).

We further investigated the solution sensitivity of AtLEA4-5 *in vitro*. We used the FRET efficiency of purified full-length AtLEA4-5 fused to mCerulean3 and mCitrine as a proxy for the end-to-end distance of the construct under different solution conditions. We induced macromolecular crowding with solutions of different molecular weight polyethylene glycol (PEG) isoforms at various concentrations, and compared these results to a previously reported macromolecular crowding biosensor (CS) as a reference (Boersma et al., 2015). The CS sensory domain is a synthetic, helical peptide with a hinge-like topology thought to compact in response to higher macromolecular crowding. Our experiments showed that PEG induced the compaction of AtLEA4-5 in a concentration and size-dependent manner (Figure 2B and Figure S4). The PEG-induced compaction was more prominent in AtLEA4-5 than in CS, confirming the relative sensitivity of AtLEA4-5 to macromolecular crowding. Together, these data show that despite its intrinsic disorder, the conformational ensemble of AtLEA4-5 is highly responsive to changes in the chemical composition of the solution, particularly macromolecular crowding, *in silico* and *in vitro*, and that these properties are based on both topology and amino acid sequence.

SED1 can dynamically track the effects of osmotic stress on live yeast cells.

We renamed the transgene expressing AtLEA4-5 to *SENSOR EXPRESSING DISORDERED PROTEIN 1* (*SED1*); "sed" translates into "thirst" in Spanish. When live yeast cells expressing SED1 were treated with NaCl and followed over time, we found that the FRET response was fast and reversible, and allowed the acclimation of yeast cells to be measured over time after hyperosmotic shock (Figure 2C). We then analyzed SED1 performance as an osmotic/crowding biosensor using CS as reference *in vivo*. We found that the dynamic range of SED1 was larger than that of CS (Figure 2D), possibly due to differences in the conformational change mechanism. This is consistent with our observations *in vitro* (Figure 2B).

To further validate the sensitivity of our biosensor *in vivo*, we sought to genetically interfere with a well-characterized osmo-protective response in yeast. To this end, we expressed SED1 in *hog1Δ* and *pbs2Δ* yeast KO mutant backgrounds. These mutants disrupt key components of the HOG (High-Osmolarity Glycerol) pathway, which is activated in yeast to respond and acclimate to increased osmolarity of the surrounding medium (Hohmann, 2009). Pbs2 is a scaffold MAPKK that integrates the two branches of the HOG pathway (Maeda et al., 1995). Hog1 is a MAPK that, upon hyperosmotic shock, translocates to the nucleus to activate transcription factors that induce genes required to promote osmoprotectant glycerol accumulation and osmotic acclimation (Rep et al., 2000). Yeast mutants of these genes are sensitive to hyperosmotic stress and cannot appropriately acclimate to these conditions (Klipp et al., 2005). When measured a few seconds after treatment with concentrations lower than 1 M NaCl, SED1 FRET ratio was larger in *hog1Δ* and *pbs2Δ* mutants than in the wild type (WT) (Figure 2E). The opposite occurred when the NaCl concentration was higher than 1 M. Since wild type cells respond and acclimate faster than the mutants under mild hyperosmotic shock (<1 M NaCl), our data

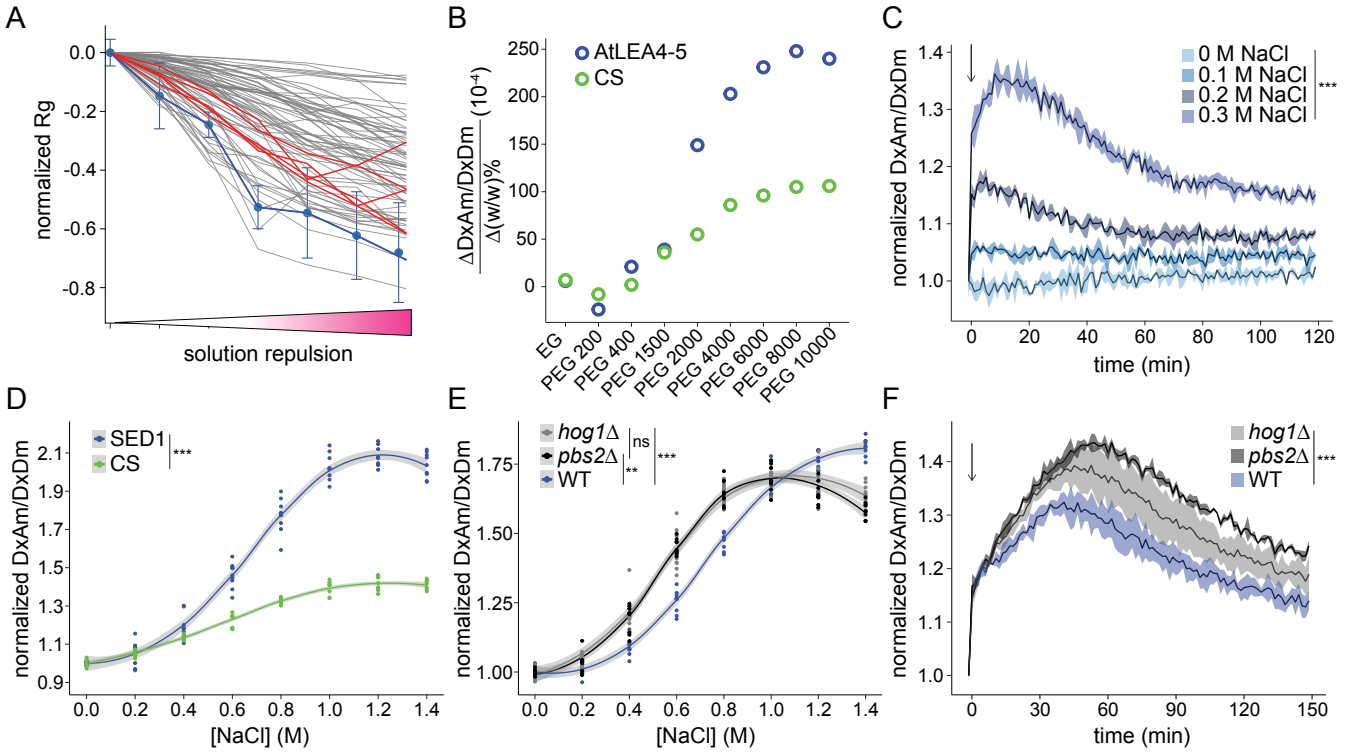

Figure 2. SED1 can dynamically track the effects of osmotic stress on live yeast cells. (A) Simulations of the normalized radius of gyration (Rg) of AtLEA4-5 (blue), five different scrambled sequences shown in Figures 1E and 1F (red), and 70 different naturally occurring IDRs (gray) under different solution repulsion levels (low to high solution repulsion of the protein backbone). Error bars are SD from 5 independent simulations. (B) FRET ratio rate of change (10^{-4}) as a function of different molecular weight osmolytes concentration (% w/w) for purified full-length recombinant AtLEA4-5 (blue) or CS (green). EG: Ethylene glycol. PEG: Polyethylene glycol. Numbers represent the average molecular weight of each type of PEG. (C) Normalized FRET ratio (DxAm/DxDm) time course of live yeast cells expressing SED1, treated with different concentrations of NaCl. The arrow indicates the addition of the treatment. Mean ± SEM. One-way ANOVA. *p < 0.05, **p < 0.01, ***p < 0.001. (D) Normalized FRET ratio (DxAm/DxDm) of live yeast cells expressing SED1 (blue) and CS (green), treated with different concentrations of NaCl. One-way ANOVA. *p < 0.05, **p < 0.01, ***p < 0.001. (E) Normalized FRET ratio (DxAm/DxDm) of wild type BY4742 strain (blue), *hog1Δ::G418* mutant (gray), and *pbs2Δ::G418* mutant (black), live yeast cells expressing SED1, hyperosmotically shocked with different concentrations of NaCl. Measurements were done immediately after hyperosmotic shock. Two-way ANOVA. *p < 0.05, **p < 0.01, ***p < 0.001. (F) Normalized FRET ratio (DxAm/DxDm) time course of wild type BY4742 strain (blue), *hog1Δ::G418* mutant (gray), and *pbs2Δ::G418* mutant (black), live yeast cells expressing SED1, treated with 0.6 M sorbitol. The arrow indicates the addition of the treatment. Mean ± SEM. Two-way ANOVA. *p < 0.05, **p < 0.01, ***p < 0.001.

suggests that SED1 response reflects the decrease in intracellular osmolarity/crowding resulting from the acclimation process.

Next, we followed the SED1 FRET ratio over time in the different backgrounds after hyperosmotic shock with 0.6 M sorbitol. As expected, we observed an immediate increase in SED1 FRET ratio upon hyperosmotic shock in all the genotypes; however, in contrast to the wild type, the mutants displayed a sustained increase in FRET before declining (Figure 2F), consistent with the reduced ability of these genotypes to acclimate. This data underscores the sensitivity of SED1 to osmotic stress in cells and suggests that it can be used to characterize the physiological effects of genetic mutants disrupting well-studied and novel osmotic stress response pathways.

Tracking SED1 response to osmotic stress in single cells reveals that vacuoles buffer against water loss

Single-cell measurements allow researchers to resolve the heterogeneity that arises in cell populations. The power of single-cell genomics has revealed cell-type-specific responses to a variety of molecular and physiological responses (Camp et al., 2019). New molecular tools that allow single-cell resolution will pave the way for unraveling currently overlooked biological mechanisms. Fluorescence biosensors are intrinsically suitable for investigating biological processes with single-cell resolution using confocal microscopy, so we aimed to investigate the performance of SED1 in individual cells. We observed that the FRET ratio in individual cells increased when they were treated with 0.5 M NaCl, in agreement with our population measurements (Figures 3A and 3B and Figure 1B). Interestingly, the FRET ratio varied between cells, even under non-stress conditions (Figures 3A and 3B), and correlated with sensor expression (Figure S5A).

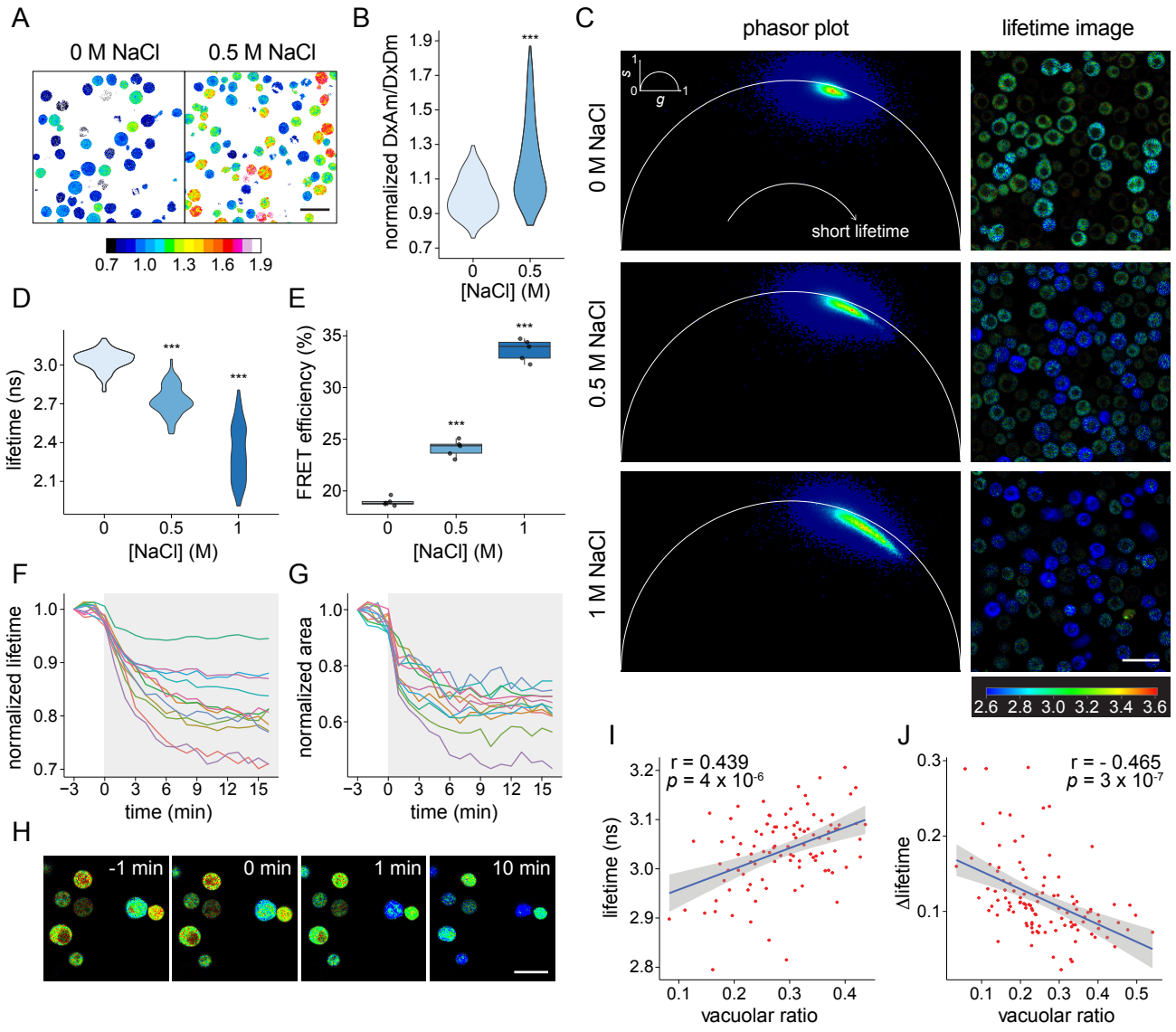

Figure 3. Tracking SED1 response to osmotic stress in single cells reveals vacuoles buffer against water loss. (A) Ratiometric image of live yeast cells expressing SED1 under 0 M and 0.5 M NaCl. Scale bar = 10 μm. Calibration bar represents the normalized FRET ratio (DxAm/DxDm). (B) Quantification of (A). Student's t-test. *p < 0.05, **p < 0.01, ***p < 0.001. (C) Phasor plots (left) and donor fluorescence lifetime images (right) of live yeast cells expressing SED1 under 0 M, 0.5 M, and 1 M NaCl. Signals shifted to the left side of the phasor plot represent longer fluorescence lifetimes, whereas signals shifted to the right side represent shorter fluorescence lifetimes. Scale bar = 10 μm. Calibration bar represents the donor fluorescence lifetime in nanoseconds (ns). (D) Quantification of the donor fluorescence lifetime of individual cells from images in (C). n = 100 cells per treatment. One-way ANOVA. *p < 0.05, **p < 0.01, ***p < 0.001. (E) FRET efficiencies of live yeast cells from images in (C). One-way ANOVA. *p < 0.05, **p < 0.01, ***p < 0.001. (F) Normalized donor fluorescence lifetime measured for single cells after 1 M NaCl treatment (shaded area) in a time course. (G) Normalized area measured for single cells after 1 M NaCl treatment (shaded area) in a time course (same cells as in (F)). The same color represents the same cell for (F) and (G). (H) Individual time frames showing the donor fluorescence lifetime of single yeast cells exposed to 1 M NaCl treatment at time 0 min. Scale bar = 10 μm. The calibration bar is the same as in (C). (I) Pearson's correlation of donor lifetime and vacuolar ratio values for single yeast cells under standard conditions (0 M NaCl). Pearson's correlation coefficient r = 0.439, p-value = 4 x 10^{-6}. (J) Pearson's correlation of the change in donor lifetime (**Δ**lifetime) and vacuolar ratio values for single yeast cells subjected to 1 M NaCl. **Δ**lifetime = (final lifetime - initial lifetime)/initial lifetime. Pearson's correlation coefficient r = - 0.465, p-value = 3 x 10^{-7}.

These data suggested that sensor expression, and overall protein concentration, may correlate with molecular crowding in the cell. In support of this hypothesis, experiments using purified SED1 found no correlation between SED1 concentration and FRET ratio *in vitro* (Figure S5B).

We also observed that SED1 protein localization was altered by hyperosmotic stress treatment. SED1 was homogeneously distributed throughout the cytoplasm under standard conditions, and rapidly re-distributed into spherical-shaped granules under 0.5 M NaCl (Figure S5C). However, the hyperosmotic-induced FRET ratio increase was not

caused by the formation of SED1 granules, since treatment with 1,6-hexanediol, a compound often used to dissociate liquid-like condensates (Kroschwald et al., 2017), dissociated the SED1 granules but did not decrease the FRET response (Figures S5D and S5E).

To further confirm that the response of SED1 to hyperosmotic stress was caused by *bona fide* donor-to-acceptor FRET, we performed fluorescence lifetime imaging-FRET (FLIM-FRET) experiments. FLIM is not sensitive to fluctuations in biosensor concentration, shading, excitation intensity, or background noise caused by the light source (Ranjit et al., 2018). In FLIM-FRET experiments, the lifetime of the donor fluorophore is effectively decreased when it undergoes FRET with the acceptor (Ranjit et al., 2018). AtLEA4-5 fused to mCerulean3 (donor-only control) expressed in yeast cells under non-stress conditions had an average fluorescence lifetime of 3.54 ± 0.10 nanoseconds (ns) (Figure S6). The average fluorescence lifetime of mCerulean3 in the SED1 construct under non-stress conditions was 3.04 ± 0.10 ns, indicating a basal FRET efficiency of 18.93% (Figures 3C-3E). Such basal FRET efficiency is comparable to the 22.93% obtained for the whole population assay, calculated using fluorescence intensities. Hyperosmotic shocks with increasing concentrations of NaCl induced a progressive shift of the cell population to shorter fluorescence lifetimes, reaching an average of 2.14 ± 0.21 ns and an average FRET efficiency of 33.63% under 1 M NaCl (Figure 3C-3E). Time-lapse imaging of individual SED1-expressing cells revealed that the drop in fluorescence lifetime occurs concomitantly with the reduction of cell volume caused by hyperosmotic shock (Figures 3F-3H and Video S1), demonstrating the fine temporal resolution capabilities of SED1 and confirming its donor-to-acceptor FRET behavior.

We further investigated the cellular basis for FRET heterogeneity among cells (Figures 3A-3D). We observed that cells with large visible vacuoles tend to have longer donor lifetimes under non-stress conditions (Figure 3C). To confirm this, we quantified the vacuolar ratio per cell, that is, the proportion of the total cell area that is occupied by the vacuole (vacuolar ratio = vacuole area/cell area). We found that the vacuolar ratio had a significant positive correlation with the donor fluorescence lifetime even in the absence of stress (Figure 3I). No correlation was observed between the cell area and donor lifetime, confirming the dominant effect of the vacuolar ratio over the FRET signal of SED1 (Figure S7A). We then measured the magnitude of the SED1 FRET change in individual cells upon hyperosmotic stress using time-lapse imaging. We found that neither the initial cell area nor the magnitude of cell area change predicted the fluorescence lifetime change after stress (Figures S7B and S7C). Strikingly, however, we observed a significant negative correlation between the change in fluorescence lifetime after treatment and the vacuolar ratio before stress (Figure 3J), suggesting that large vacuoles might effectively buffer water loss during hyperosmotic shock. Overall, the use of SED1 revealed how rapid cell-specific changes in the osmotic status of cells are well correlated to intracellular features such as relative vacuolar size. Furthermore, our data demonstrates the importance of measuring physical-chemical properties at the single-cell level for obtaining mechanistic insights of cellular homeostasis.

SED1 tracks changes in osmolarity in a wide set of organisms.

Given the ability of SED1 to report the effects of osmotic stress on budding yeast, we sought to apply it to other biological systems. We first expressed SED1 in the bacteria *Escherichia coli*. Similar to what we found in yeast, we observed a hyperosmotic stress-dependent increase in the FRET readout (Figure 4A and Figure S8A). Next, we tested SED1 in two evolutionarily distant multicellular organisms: plants and humans.

Plants heavily rely upon water to provide structural support and to facilitate gas exchange with the environment (Scharwies and Dinneny, 2019). To test the utility of SED1 in this context, we transiently expressed a nuclear-localized SED1 transgene in tobacco leaves. Small discs of leaf tissue were placed onto 96-well plates, in wells containing hyperosmotic (sorbitol or NaCl) or hypoosmotic (water) solutions. We found that when SED1-expressing leaf discs were incubated with sorbitol or NaCl, the FRET readout increased over time (Figure 4B), with an increase in fluorescence intensity of the acceptor and a concomitant decrease in fluorescence of the donor (Figures S8B and S8C). On the other hand, when leaf discs were treated with pure water, the opposite behavior in fluorescence intensities was observed (Figure 4B and Figure S8D). These results indicate that SED1 is functional in multicellular photosynthetic organisms and encouraged us to further characterize SED1 in *Arabidopsis thaliana* transgenic lines. 5-day-old Arabidopsis seedlings expressing *pUBQ10::nlsSED1* were imaged on a Murashige & Skoog (MS)-agar media pad before and after the addition of a solution containing 0.5 M NaCl. Contrary to what we observed in *N. benthamiana*, we did not observe hyperosmotic-dependent FRET ratio changes in any of the cells analyzed (Figure S9). Since AtLEA4-5 - the sensory domain of SED1 - is an Arabidopsis protein, the lack of response could be the result of its interaction with endogenous binding partners and/or posttranslational modifications. In agreement with the latter hypothesis, it was recently reported that LEA proteins are hyper-phosphorylated at almost every serine, threonine, and tyrosine residue in Arabidopsis (Mergner et al., 2020). The introduction of several negative charges throughout the protein likely prevents hyperosmotic stress-induced compaction.

We further tested SED1 in human cells. To do so, we stably introduced SED1 into human epithelial (U-2 OS) cells and measured the SED1 FRET signal in response to sorbitol

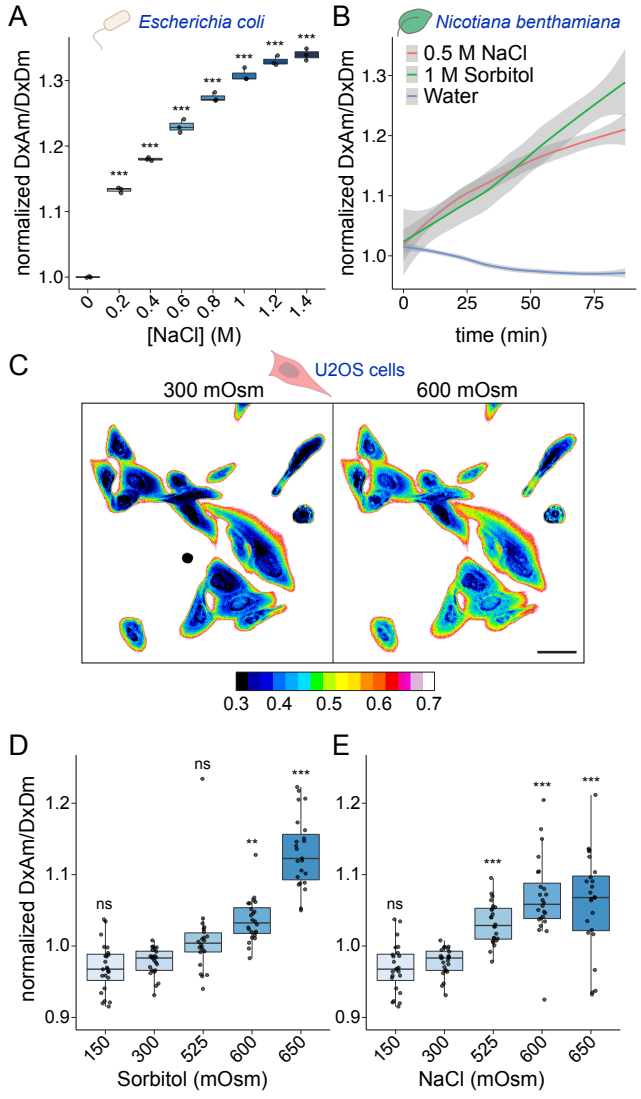

Figure 4. SED1 tracks changes in osmolarity of a wide set of organisms. (A) Normalized FRET ratio (DxAm/DxDm) of live SED1-expressing *Escherichia coli* cells treated with different concentrations of NaCl. One-way ANOVA. *p < 0.05, **p < 0.01, ***p < 0.001. (B) Normalized FRET ratio (DxAm/DxDm) time course of *Nicotiana benthamiana* leaf discs transiently expressing SED1, treated with either water, 0.5 M NaCl, or 1 M sorbitol. n = 12 leaf discs. Mean ± SEM. One-way ANOVA. (C) Ratiometric image of live SED1-expressing U-2 OS cells at 300 mOsm (isosmotic) or 600 mOsm (hyperosmotic) treated with sorbitol. Scale bar = 50 μm. Calibration bar represents the normalized FRET ratio (DxAm/DxDm). (D) Normalized FRET ratio of SED1-expressing U-2 OS cells exposed to different osmotic treatments with sorbitol. (E) Normalized FRET ratio of SED1-expressing U-2 OS cells exposed to different osmotic treatments with NaCl. One-way ANOVA. *p < 0.05, **p < 0.01, ***p < 0.001.

and NaCl treatments at different osmolarities using live-cell confocal microscopy. We observed that both treatments induced an increased FRET ratio immediately after the addition of the solution (Figures 4C-4E). The increased fluorescence of the acceptor and decreased fluorescence of the donor after the treatments, along with the acceptor photobleaching control, confirmed the expected FRET behavior (Figure S10). This data demonstrates that SED1 is responsive in live human cells.

In conclusion, we showed that SED1 is a versatile, genetically-encoded optical tool that can be used to dynamically track the response to osmotic stress of living cells from a plethora of organisms in an inherently quantitative manner. This opens new avenues to investigate the poorly-understood impact of environmental perturbations on the regulation of cellular function.

DISCUSSION

Recent progress in the characterization of the molecular and cellular functions of IDRs has revolutionized our understanding of cell biology. Protein domains that lack a defined and stable structure perform important functions including signalling, transcriptional and translational regulation, stress protection, and control of enzymatic function (Bah and Forman-Kay, 2016; Boothby et al., 2017; Keul et al., 2018; Tompa, 2005; Van Roey et al., 2014). Dysregulation of IDR-containing proteins (like TP53, alpha-synuclein, and TDP-43) often results in disease (Uversky et al., 2008). IDRs are key players in the process of liquid-liquid phase separation (LLPS), which is thought to mediate the formation of intracellular membraneless compartments such as the nucleolus (Shin and Brangwynne, 2017). Notably, the dynamic conformational structure of IDRs can be modulated by interaction with binding partners, posttranslational modifications, or changes in the chemical environment of the solution (Cuevas-Velazquez et al., 2016; Moses et al., 2020; Wright and Dyson, 2015). Despite this significant progress in understanding the functions of IDRs, their potential for building molecular tools such as biosensors has been largely overlooked. Here, we leverage the unique features of IDRs to develop a highly sensitive biosensor that exploits the flexible nature and sensitivity to osmolarity changes of a plant IDR. Because of the unique capabilities mentioned above and the high prevalence of IDRs in the proteomes of organisms across all kingdoms of life, we anticipate that this work will pave the way for using IDRs to develop cutting-edge molecular tools.

SED1 can dynamically monitor the effects of osmotic stress in *Escherichia coli*, *Saccharomyces cerevisiae*, *Nicotiana benthamiana*, and human cells. In contrast, SED1 was not responsive in *Arabidopsis thaliana*. Since the sensory domain of SED1 (AtLEA4-5) is an Arabidopsis protein, we hypothesize that the environmentally-driven conformational changes might be affected by interaction with its endogenous binding partners, or by post-translational modifications, as recently shown for other LEA proteins (Mergner et al., 2020). Tuning SED1 sequence to make it sufficiently different from endogenous AtLEA4-5 while maintaining its environmental responsiveness would be the next step for using this biosensor in plants. The use of computational solution space scanning

will likely aid in these efforts as the role of individual amino acid variants can be tested.

SED1 has a larger dynamic range than the macromolecular crowding biosensor (CS) (Boersma et al., 2015). The CS sensory domain is a synthetic peptide composed of two α-helices in a hinge-like topology. AtLEA4-5 is a naturally occurring IDP that lacks secondary structure, yet exhibits a more dramatic response to increased macromolecular crowding than CS both *in vitro* and *in vivo*. It is important to note that the disorder levels and amino acid content of the protein are not sufficient to explain this dramatic response to changing cellular conditions, since all the different scrambled versions of AtLEA4-5 we tested had a decreased ability to compact (Figures 1F and 2A). Therefore, the primary sequence, and the intramolecular interactions they facilitate in AtLEA4-5, form the molecular underpinnings for the stress-induced compaction observed *in vivo*, supporting our previous evidence *in vitro* (Cuevas-Velazquez et al., 2016). Indeed, the sensitivity of IDRs to their physical-chemical environment has been shown to be sequence dependent, and might regulate their function, as proposed previously (Moses et al., 2020). The functional regulation of disordered domains by environmental factors could have enormous implications, especially for organisms with high content of IDPs in their proteome. This work contributes to a better understanding of how the primary sequence of disordered regions accounts for their sensitivity to the physical-chemical properties of the environment in cells.

Single budding yeast cells expressing SED1 displayed different FRET levels under non-stress conditions and may be due to variation in protein concentration and overall macromolecular crowding in cells. Additional variation in the population was observed upon hyperosmotic shock where cells with larger vacuoles showed a smaller change in FRET after treatment. Vacuoles serve as a reservoir of water and allow cells to lose water under hyperosmotic stress without dramatically changing the concentration of solutes in the cytoplasm. Whether other vacuole-containing organisms such as plants display similar variation in SED1 FRET levels remains to be studied and opens the possibility for understanding how cells cope with different water availability through the use of intracellular compartments.

The use of SED1 to monitor osmotic variations in living cells has the potential to reveal new fundamental aspects of cell biology. SED1 might be used to 1) dynamically track the macromolecular crowding of individual cells during perception, response, and acclimation to osmotic stress; 2) screen for mutants disrupted in the sensing and response mechanisms to osmotic shock; 3) test whether other kinds of stressors induce intracellular osmotic variation; 4) generate osmolarity and/or macromolecular crowding maps of different cell types of multicellular organisms. This has the potential to revolutionize our understanding of the biological processes that enable desiccation survival, extreme salt tolerance, and rehydration. The ability of SED1 to work in evolutionarily distant organisms means that these processes can be studied across the tree of life to broaden our understanding of the ways in which water regulates life on earth.

ACKNOWLEDGEMENTS

We thank members of the Dinneny lab for critical review of the manuscript; members of the Carnegie-Stanford Intrinsically Disordered Proteins Scientific Interest Group (IDPSIG) for helpful discussions and for fostering important collaborations for this manuscript; Heather Cartwright for technical assistance in confocal microscopy; Shouling Xu for assistance with FPLC; Dr. Hugo Tapia for providing wild type BY4742 strain as well as *hog1Δ::G418* and *pbs2Δ::G418* mutants; Dr. Arnold Boersma for providing Cr1-pRSET-A plasmid; Dr. Wolf B. Frommer for providing pGW1araF.Ec plasmid; and Dr. Cindy Ast for providing pGPTVII-Bar-U-MCaMP6s plasmid.

C.L.C.V. was a Latin American Fellow in the Biomedical Sciences, supported by the Pew Charitable Trusts. The research of J.R.D. was supported in part by a Faculty Scholar grant from Howard Hughes Medical Institute and the Simons Foundation. We gratefully acknowledge computing time on the MERCED cluster at UC Merced, funded by NSF grant No. ACI-1429783, and on the XSEDE computational infrastructure framework, grant No. TG-MCB190103 to S.S., supported by NSF grant No. ACI-1548562. S.S., D.M., and F.Y. were supported by the NIH under award R35GM137926 to S.S.; D.M. and K.G. were supported by a fellowship from NSF-CREST Center for Cellular and Biomolecular Machines at UC Merced, grant No. NSF-HRD-1547848.

AUTHOR CONTRIBUTIONS

Conceptualization, C.L.C.V., A.A.C., and J.R.D.; Methodology, C.L.C.V., J.A.N.B., S.S., and J.R.D.; Software, F.Y., and S.S.; Formal Analysis, C.L.C.V., T.V., F.Y., and S.S.; Investigation, C.L.C.V., T.V., K.G., H.B.S., F.Y., D.M., J.A.N.B., D.C.A., A.D., and L.W.; Resources, A.M.J.; Writing - Original Draft, C.L.C.V. and J.R.D.; Writing - Review & Editing C.L.C.V., T.V., K.G., H.B.S., D.M., J.A.N.B., A.D., A.M.J., A.A.C., S.S., J.R.D.; Visualization, C.L.C.V., T.V., and S.S., Supervision, C.L.C.V., A.A.C., S.S., and J.R.D.; Funding Acquisition, C.L.C.V., A.A.C., S.S., and J.R.D.

DECLARATION OF INTERESTS

The authors declare no competing interests.

MATERIAL AND METHODS

All-atom simulation

Simulations of AtLEA4-5 protein, its scrambles, and other IDRs were done using Solution Space Scanning (Holehouse and Sukenik, 2020), an all-atom Monte Carlo simulation method based on the ABSINTH force field (Mittal et al., 2014; Vitalis and Pappu, 2009) that has been previously described

(Holehouse and Sukenik, 2020). Briefly, the Hamitonian function to be evaluated in each step can be written as the following representation.

$$E_{total} = W_{solv} + U_{LJ} + W_{el} + U_{corr}$$

Here, W_{solv} is the energy describing the interaction between the protein surface and the surrounding solution. By changing the W_{solv} term, we can alter this interaction and sample a protein's conformations in different solution conditions.

For each combination of solution condition and protein (AtLEA4-5 and each of its sequence scrambles), we ran five independent simulations consisting of $5x10^7$ Monte Carlo steps (following $1x10^7$ steps of equilibration) starting from random conformations to ensure proper sampling. Protein conformations were written out every 12,500 steps. The dataset of 70 other IDRs shown in Fig. 2A was obtained using the same methods, is publicly available on https://github.com/sukeniklab/HiddenSensitivity, and has been previously described (Moses et al., 2020). We analyzed the average radii of gyration of the simulated conformation ensembles using the MDTraj python library (McGibbon et al., 2015). Standard deviations were calculated based on the average of five individual repeats. Each radius of gyration was then normalized based on the most expanding solution to highlight solution sensitivity.

Transgene constructs

pDRFLIP38 backbone was used for biosensors yeast expression (Jones et al., 2014). This plasmid contains the constitutive promoter pPMA1, and was provided by Dr. Alexander M. Jones. The vector was digested with XbaI (NEB) and EcoRI (NEB) to clone the open reading frames (ORFs) of mCreluan3, AtLEA4-5, and mCitrine downstream of the pPMA1 promoter. The biosensor construct was cloned using the Gibson Assembly cloning method (NEB) by mixing the XbaI-EcoRI-digested pDRFLIP38 with the PCR-amplified ORFs containing overlapping ends. The ORFs of the other fluorescent proteins (t7.eCFP.t9, Aphrodite.t9, t7.TFP.t9, mTFP.t9, Cerulean, Citrine, edCerulean, edCitrine, edAphrodite.t9) used in this study were cloned in the same way. The sensory domains tested (AtLEA4-2, ABP, CS, N-AtLEA4-5, C-AtLEA4-5, Scramble-1, Scramble-2, Scramble-3, Scramble-4, Scramble-5) were cloned between mCerulean3 and mCitrine ORFs. To do this, pDRFLIP38-AtLEA4-5 was digested with SacI and BglII to remove the AtLEA4-5 ORF. The digested plasmid was mixed with the different PCR-amplified sensory domains-ORFs containing overlapping ends using the Gibson Assembly method (NEB). AtLEA4-2, AtLEA4-5, N-AtLEA4-5, and C-AtLEA4-5 ORFs were amplified from pTrc99A-AtLEA4-2 and pTrc99A-AtLEA4-5 plasmids provided by Dr. Alejandra A. Covarrubias (Cuevas-Velazquez et al., 2016). ABP ORF was amplified from pGW1araF.Ec plasmid provided by Dr. Wolf B. Frommer (Kaper et al., 2008). CS ORF was amplified from Cr1-pRSET-A provided by Dr. Arnold Boersma (Boersma et al., 2015). All AtLEA4-5 Scrambled ORFs were synthesized as gene fragments (Genscript).

For bacterial expression, pDEST-HisMBP backbone was used (Addgene #11085). This plasmid contains the Tac IPTG-inducible promoter for protein expression with a N-terminal 6x His tag and an MBP tag. The full SED1 ORF was cloned into pENTR-D-TOPO (Thermo Fisher Scientific). Recombination of pENTR-D-TOPO-SED1 and pDEST-HisMBP was done using Gateway technology to produce pDEST-HisMBP-SED1. The same strategy was followed for the full CS ORF to produce pDEST-HisMBP-CS.

pGPTVII-Bar-U-MCaMP6s binary vector was used for expression in plant cells (Ast et al., 2017). This plasmid contains the AtUBQ10 promoter, and was provided by Dr. Cindy Ast. The plasmid was digested with SpeI (NEB) and XmaI (NEB). SED1 was cloned using the Gibson Assembly cloning method (NEB) by mixing the SpeI-XmaI-digested pGPTVII-Bar-U-MCaMP6s with the PCR-amplified SED1 ORF containing overlapping ends. The nuclear localization signal was added in the forward primer (ATGCTGCAGCCTAAGAAGAAGAGAAAGGTTGGAGGG).

Transgene expression

The constructs indicated in the main text were transformed into *Saccharomyces cerevisiae* protease-deficient yeast strain (BJ5465 lacking Pep4 and Prb1) using the lithium acetate transformation method (Daniel Gietz and Woods, 2002). Transformed colonies were selected in plates containing 6.8 g/L YNB media (Sigma-Aldrich) supplemented with 5 g/L glucose and 1.92 g/L synthetic drop-out medium without uracil (Sigma-Aldrich). Positive clones were confirmed by colony PCR. SED1 was also transformed into wild type and *hog1Δ::G418* and *pbs2Δ::G418* mutant backgrounds of the *Saccharomyces cerevisiae* BY4742 strain (provided by Dr. Hugo Tapia). Transformation and selection was done as described above.

pDEST-HisMBP-SED1 was transformed into *Escherichia coli* BL21 (DE3) strain using the heat shock transformation method. Transformed colonies were selected in plates containing LB media supplemented with ampicillin (100 µg/mL). Positive clones were confirmed by colony PCR. The same strategy was followed for pDEST-HisMBP-CS.

pGPTVII-nlsSED1 was transformed into *Agrobacterium tumefaciens* GV3101 (pSoup) strain using the electroporation method. Transformed colonies were selected in plates containing LB media supplemented with gentamicin (50 µg/mL), kanamycin (50 µg/mL), and tetracycline (2 µg/mL). Positive clones were confirmed by colony PCR. For transient expression in *Nicotiana benthamiana*, the positive *Agrobacterium tumefaciens* clones and p19 strain were co-transfected in large *Nicotiana benthamiana* leaves and incubated for 5 days before measurements (Li, 2011). For

stable expression in Arabidopsis thaliana, four pots of 30 days-after-sowing (flowering) Col-0 plants were transformed with the positive *Agrobacterium tumefaciens* clones using the floral dip method (Zhang et al., 2006). T1 transformed seeds were selected in MS media containing DL-Phosphinothricin herbicide. Three independent T3 homozygous plants were selected for imaging.

Fluorescence analysis of live *Saccharomyces cerevisiae* cells

5 mL of yeast cells expressing the indicated constructs (see main text) were grown at 30°C in liquid YNB media (6.8 g/L) (Sigma-Aldrich) supplemented with 5 g/L glucose and 1.92 g/L synthetic drop-out medium without uracil (Sigma-Aldrich) until OD600 ~ 1 – 2. Cells were centrifuged and washed twice with 50 mM MES, pH 6 and resuspended in 5 mL of the same buffer. 50 µL of the cell suspension was loaded into individual wells of a 96-well black F-bottom clear microplate (Greiner). 150 µL of treatment solution (see main text) was added to the cell suspension, mixing was performed by pipetting up and down, and the fluorescence was measured immediately after. Fluorescence readings were acquired using a Safire fluorimeter (Tecan) for donor fluorophore (mCerulean3 excitation 433 nm, mCerulean3 emission 480 nm, abbreviated DxDm), acceptor fluorophore (mCitrine excitation 510 nm, mCitrine emission 525 nm, abbreviated AxAm), and energy transfer from donor to acceptor (mCerulean3 excitation 433 nm, mCitrine emission 525 nm, abbreviated DxAm). Fluorescence emission scans from 460 nm to 550 nm (step size 5 nm) with an excitation wavelength of 433 nm were acquired. For all fluorescence measurements, bandwidth was set to 5 nm (7.5 nm for the emission scan), number of flashes was 10, integration time was 40 µs, and gain was 100. For time course measurements, the 96-well plate was kept inside the plate reader for the duration of the experiment. Measurements were acquired every 60 seconds for a period of 120 to 150 minutes. Shake (linear) duration was set to 3 seconds before every measurement. Three independent experiments were carried out for each construct, and three technical replicates for each treatment.

Fluorescence analysis of live *Escherichia coli* cells

3 mL of SED1-expressing *Escherichia coli* culture was grown at 37°C in liquid LB supplemented with ampicillin to OD600 ~ 1 – 2. No IPTG induction was needed since the fluorescence obtained from the leaking expression of the Tac promoter was sufficient for measurements. Cells were centrifuged and washed twice with 50 mM MES, pH 6 and resuspended in 3 mL of the same buffer. 50 µL of the cell suspension was loaded into individual wells of a 96-well black F-bottom clear microplate (Greiner). 150 µL of treatment solution (see main text) was added to the cell suspension, mixing was performed by pipetting up and down, and the fluorescence was measured immediately after. Fluorescence readings were acquired using a Safire fluorimeter (Tecan) for donor fluorophore (mCerulean3 excitation 433 nm, mCerulean3 emission 480 nm, abbreviated DxDm), acceptor fluorophore (mCitrine excitation 510 nm, mCitrine emission 525 nm, abbreviated AxAm), and energy transfer from donor to acceptor (mCerulean3 excitation 433 nm, mCitrine emission 525 nm, abbreviated DxAm). Fluorescence emission scans from 460 nm to 550 nm (step size 5 nm) with an excitation wavelength of 433 nm were acquired. For all fluorescence measurements, bandwidth was set to 7.5 nm, number of flashes was 10, integration time was 40 µs, and gain was 100. Three independent experiments were carried out with three technical replicates for each treatment.

Fluorescence analysis of live *Nicotiana benthamiana* cells

Nicotiana benthamiana leaf discs were obtained from leaves transiently expressing SED1 and loaded into individual wells of a 96-well black F-bottom clear microplate (Greiner). 5 µL of water was added to the bottom of the well before loading the leaf discs to facilitate a flattened distribution of the leaf to the bottom of the well. 20 µL of the indicated solution (see main text) was added to the top of each leaf disc and fluorescence was measured immediately after. The 96-well plate was kept inside the plate reader for the duration of the experiment. Measurements were acquired every 180 seconds for a period of 90 minutes. Shake (linear) duration was set to 3 seconds before every measurement. Fluorescence readings were acquired using a Safire fluorimeter (Tecan) for donor fluorophore (mCerulean3 excitation 433 nm, mCerulean3 emission 480 nm, abbreviated DxDm), acceptor fluorophore (mCitrine excitation 510 nm, mCitrine emission 525 nm, abbreviated AxAm), and energy transfer from donor to acceptor (mCerulean3 excitation 433 nm, mCitrine emission 525 nm, abbreviated DxAm). For all fluorescence measurements, bandwidth was set to 5 nm, number of flashes was 10, integration time was 40 µs, and gain was 100. Three independent experiments were carried out with 12 leaf discs for each treatment.

Saccharomyces cerevisiae fluorescence microscopy

5 mL of yeast cells expressing the indicated constructs (see main text) were grown at 30°C in liquid YNB media (6.8 g/L) (Sigma-Aldrich) supplemented with 5 g/L glucose and 1.92 g/L synthetic drop-out medium without uracil (Sigma-Aldrich) until OD600 ~ 1 – 2. Cells were centrifuged and washed twice with 50 mM MES, pH 6 and resuspended in 5 mL the same buffer. 100 µL of the cell suspension was loaded into a µ-Slide 8-well Ibidi chamber (Ibidi GmbH) and mixed with 100 µL of the treatment solution (2X) to reach the desired final concentration (see main text). Imaging was done immediately after the treatment.

Imaging was performed with a Leica TCS SP8 laser scanning confocal microscope with LASX software. For intensity-based measurements a 63x/1.4 NA oil HCX PL APO immersion objective was used for all the experiments. Thirty

Z-stack images with steps of 0.3 µm (system optimized) were captured. Three kinds of images were acquired in sequential mode for each experiment: donor emission with donor excitation (DxDm; donor channel), acceptor emission with donor excitation (DxAm; FRET channel), and acceptor emission with acceptor excitation (AxAm; acceptor only channel). For DxDm, excitation = 440 nm; emission = 450 - 500 nm. For DxAm, excitation = 440 nm; emission = 525 - 550 nm. For AxAm, excitation = 514 nm; emission = 525 - 550 nm. Laser power was set between 2-5% and detector gain was set to 80. At least three different fields of view were acquired for each strain/treatment. Fluorescence emission was detected by HyD detectors. A line average of eight was used for all the experiments.

For 1,6-hexanediol treatment, only AxAm was followed. Cells were first treated with 0.5 M NaCl and subsequently incubated with 10% (w/v) 1,6-hexanediol. Imaging was done at the parameters indicated above.

FLIM-FRET experiments were carried out on yeast strains containing AtLEA4-5-mCerulean3 (donor-only) and SED1 (donor and acceptor: mCerulean3 and mCitrine). FLIM was measured using a Leica TCS SP8 FALCON confocal microscope with LASX software. A 93x/1.3 NA glycerin immersion objective was used for all experiments. Excitation of the donor fluorophore was done at 440 nm with a diode pulsed laser at 40 MHz repetition rate. Emission from 450-515 nm was collected with a HyD SMD hybrid detector. Laser power was adjusted to obtain ~1 photon per laser pulse, and 20 frames were integrated. The pixel frame size was set to 512, which gave a pixel size of 0.24 µm.

Saccharomyces cerevisiae image analysis

For intensity-based measurements, the images were analyzed using Fiji (http://fiji.sc/). Sum of Z-stacks and background subtraction were performed for DxAm, DxDm, and AxAm images. Regions of interest corresponding to individual cells were selected and ratios of DxAm/DxDm were calculated and normalized to the no-treatment mean. To generate the ratiometric image, Gaussian blur of 1 was applied to all images. AxAm was used to create a mask. DxAm/DxDm ratio image was multiplied by the mask image, divided by 255 and set to the same range for all images. Background was manually set to white pixels for clarity.

FLIM measurements were analyzed using LASX software. FRET efficiency was calculated for the entire image by comparing the FLIM values obtained for the mCerulian3 donor fluorophore in the presence and absence of the mCitrine acceptor fluorophore. First, the average fluorescence lifetime of the donor was determined by fitting every image with two exponential components. The resultant Mean t Amplitude Weighted value was used as the Unquenched Donor Lifetime parameter to calculate the FRET efficiency by applying a multi-exponential decay model to fit the experimental decays. For individual SED1-expressing cells, a region of interest was selected for every cell and lifetime was calculated by fitting the fluorescence decay with a single exponential model. The vacuolar ratio was calculated as the ratio between vacuole area and total area per cell. Vacuole area and total area per cell were obtained from the fluorescence intensity images using Fiji.

Protein purification

1 L of LB supplemented with ampicillin (100 µg/mL) was inoculated with 5 mL of a saturated culture of cells containing pDEST-HisMBP-SED1. The culture was grown at 37°C and 250 rpm to OD600 ~ 0.5. At this point, recombinant protein was induced with 1 mM IPTG (Sigma – Aldrich) and the culture was transferred to 25°C and 250 rpm for 5 hours. Cells were collected and lysed by sonication on ice, and the extract was clarified by centrifugation. The His-tagged recombinant fusion protein was separated by cobalt immobilized metal chelate affinity beads using the HisPur Cobalt Purification Kit (Thermo Scientific) following the procedure described by the manufacturer. To remove the His-MBP tag, the dialyzed recombinant protein was incubated at 4°C overnight with TEV protease. Tag-free recombinant SED1 was separated by FPLC (AKTA Purifier 10). Fractions containing the purified protein were combined and dialyzed against 20 mM sodium phosphate, pH 7.4, 100 mM NaCl, for further usage. The purity of recombinant SED1 was confirmed by SDS-PAGE. The same strategy was followed for pDEST-HisMBP-CS.

Solution preparation and specifics

Solutes were purchased from Alfa Aesar (PEG200, PEG400, PEG1500, PEG2000, PEG4000, PEG6000, PEG8000, PEG10000), and used without further purification. Stock solutions were made by mixing the solute with 20 mM sodium phosphate buffer, pH 7.4, with the addition of 100 mM NaCl except for NaCl and KCl solutions, which were initially free of additional salt. The same buffer was used for all dilutions.

Fluorescence analysis of purified recombinant proteins

FRET experiments were conducted in black plastic 96-well plates (Nunc) using a CLARIOstar plate reader (BMG LABTECH). Buffer, stock solution, and purified protein solution were mixed in each well to reach a volume of 150 µL containing the desired concentrations of the solute and the FRET construct, with a final concentration of 0.43 µM protein. Fluorescence measurements were taken from above, at a focal height of 5.7 mm, with gain fixed at 1020 for all samples. For each construct, 18 replicates were performed in neat buffer, and one measurement was done in every other solution condition. Fluorescence spectra were obtained for each construct in each solution condition by exciting the sample in a 10-nm band centered at λ = 433 nm, with a dichroic at λ = 446.5 nm, and measuring fluorescence emission from λ = 460 to 600 nm, averaging over a 10 nm window moved at intervals of 0.5 nm. The ratio of acceptor to donor intensity

(DxAm/DxDm) was calculated by dividing the total measured fluorescence intensities from 500 to 600 nm by the total measured fluorescence intensities from 460 to 499 nm.

U-2 OS cell culture

All U-2 OS (ATCC HTB-96) and HEK-293T (ATCC CRL-3216) cell lines used in this study were cultured at 37°C in 5% CO_2 in high-glucose DMEM (GE Healthcare) supplemented with 10% FBS (Atlanta Biologicals), 1 mM sodium pyruvate (Gibco), 2 mM L-glutamine (Gemini Biosciences), 1x MEM non-essential amino acids (Gibco), 40 U/ml penicillin and 40 µg/ml streptomycin (Gemini Biosciences). Stable U-2 OS SED1-expressing cell lines were generated by lentiviral transduction. To produce lentiviral particles, the SED1 construct was first subcloned into EcoRV-HF (NEB)-digested pLenti-CMV Puro DEST (Addgene #17452) using the NEBuilder HiFi DNA Assembly master mix (NEB), and then transfected into HEK-293T cells together with pMD2.G (Addgene #12259) and psPAX2 (Addgene #12260). Virus was harvested 48 h after transfection, filtered through non-binding 45 µm syringe filters (Pall Corporation) and used to transduce U-2 OS cells. After 24 h, the virus-containing medium was removed and replaced with selection medium containing 2 µg/ml Puromycin (Sigma–Aldrich). After 7 days of selection, single-cell clones were derived by sorting for the top ~60% fluorescent cells using a Sony SH800 flow cytometer. Two individual clones were randomly selected for further use.

U-2 OS sample preparation

U-2 OS cells expressing SED1 were cultured in Corning treated flasks with Dulbecco's modified Eagle's medium (DME:F-12 1X from Hyclone Cat No SH30023.01) supplemented with 10% FBS (Gibco REF 16000-044) and 1% penicillin/streptomycin (Gibco REF 15140-122). Cells were incubated at 37°C and 5% CO_2. Sorbitol (VWR CAS 50-70-4) and NaCl (Fisher Bioreagents CAS 7647-14-5) stock solutions of 3 M and 5 M respectively were prepared by dissolving the corresponding amounts of sorbitol or NaCl in autoclaved DI water and filtering using a 0.2 µm filter. The solutions used for perturbations were obtained by diluting the stock solutions with autoclaved DI water.

Prior to imaging, 13,000 cells were plated in a µ-Plate 96-well black treated imaging plate (Ibidi) and allowed to adhere overnight (~16 hours) before perturbations. Cells were stained with DAPI (Thermo). To prepare the stain, a 14.3 mM DAPI stock dissolved in DI water was diluted to a final concentration of 300 µM with complete media. The media from the cells was aspirated and DAPI-containing media was added to the cells, which were then incubated for 15 minutes at 37°C and 5% CO_2. After the incubation period, the cells were rinsed twice with PBS and 200 µL of PBS was added.

U-2 OS fluorescence microscopy

Imaging was done on a Zeiss epifluorescent microscope using a 40X 0.9 NA dry objective. Excitation was done with a Colibri LED excitation module and data was collected on dual Hamamatsu Flash v3 sCMOS cameras. The cells were imaged at room temperature before and less than 1 minute following perturbation with 300 ms exposure times. Imaging was done by exciting DAPI (385 nm) under donor excitation (Dx, 430 nm) or acceptor excitation (Ax, 511 nm). Emitted light was passed on to the camera using a triple bandpass dichroic (467/24, 555/25, 687/145). When measuring FRET, emitted light was split into two channels using a downstream beamsplitter with a 520 nm cutoff. For each perturbation, the cells were focused using the DAPI channel, and imaged with two channels using Dx, in one channel using Ax. The final osmolarities that were used for the perturbations were: 150 mOsm, 300 mOsm (isosmotic), 525 mOsm, 600 mOsm, and 650 mOsm with sorbitol or NaCl as the osmotic agents. From each well in the 96-well plate, 4-5 cells were analyzed. Each perturbation was replicated at least 3 times in a single plate, and the data reported are combined from at least two plates prepared on different days.

U-2 OS image analysis

The images were analyzed using ImageJ. For each cell, 5 ROIs were selected: (1) background ROI, located where no cells were present, to measure any background changes that may have occurred due to media changes; (2-5) four ROIs in the cytoplasm of each cell. For each ROI, the background signal was subtracted, and average intensity values were reported in four channels: (a) donor emission under donor excitation (DxDm), (b) acceptor emission under donor excitation (DxAm), (c) acceptor emission under acceptor excitation (AxAm), and (d) DAPI emission under DAPI excitation. To correct for donor bleedthrough, cells were plated and stained as previously mentioned. Cells were imaged, the acceptor was photobleached under prolonged direct acceptor excitation, and the cells were imaged again. ROIs of all the cells present in the plane of view were measured. A correlation plot of donor emission against acceptor emission was generated to determine percent bleedthrough, as shown in Figure S10D.

Statistical analysis

Data was analyzed with one-way ANOVA or two-way ANOVA for all experiments with more than two samples, as indicated in the figure legends, with Tukey's multiple comparison test. For experiments with two samples, data was analyzed using unpaired Student's t-test. Symbols *, **, and *** indicate p values < 0.05, 0.01, and 0.001, respectively.

REFERENCES

Ast, C., Foret, J., Oltrogge, L.M., De Michele, R., Kleist, T.J., Ho, C.-H., and Frommer, W.B. (2017). Ratiometric Matryoshka

biosensors from a nested cassette of green- and orange-emitting fluorescent proteins. Nat. Commun. *8*, 431.

Bah, A., and Forman-Kay, J.D. (2016). Modulation of Intrinsically Disordered Protein Function by Post-translational Modifications. J. Biol. Chem. *291*, 6696–6705.

Boersma, A.J., Zuhorn, I.S., and Poolman, B. (2015). A sensor for quantification of macromolecular crowding in living cells. Nat. Methods *12*, 227–229, 1 p following 229.

Boothby, T.C., Tapia, H., Brozena, A.H., Piszkiewicz, S., Smith, A.E., Giovannini, I., Rebecchi, L., Pielak, G.J., Koshland, D., and Goldstein, B. (2017). Tardigrades Use Intrinsically Disordered Proteins to Survive Desiccation. Mol. Cell *65*, 975–984.e5.

Bourque, C.W. (2008). Central mechanisms of osmosensation and systemic osmoregulation. Nat. Rev. Neurosci. *9*, 519–531.

Camp, J.G., Platt, R., and Treutlein, B. (2019). Mapping human cell phenotypes to genotypes with single-cell genomics. Science *365*, 1401–1405.

Cuevas-Velazquez, C.L., and Dinneny, J.R. (2018). Organization out of disorder: liquid–liquid phase separation in plants. Curr. Opin. Plant Biol.

Cuevas-Velazquez, C.L., Saab-Rincón, G., Reyes, J.L., and Covarrubias, A.A. (2016). The Unstructured N-terminal Region of Arabidopsis Group 4 Late Embryogenesis Abundant (LEA) Proteins Is Required for Folding and for Chaperone-like Activity under Water Deficit. J. Biol. Chem. *291*, 10893–10903.

Daniel Gietz, R., and Woods, R.A. (2002). Transformation of yeast by lithium acetate/single-stranded carrier DNA/polyethylene glycol method. In Methods in Enzymology, C. Guthrie, and G.R. Fink, eds. (Academic Press), pp. 87–96.

Greenwald, E.C., Mehta, S., and Zhang, J. (2018). Genetically Encoded Fluorescent Biosensors Illuminate the Spatiotemporal Regulation of Signaling Networks. Chem. Rev. *118*, 11707–11794.

Haswell, E.S., and Verslues, P.E. (2015). The ongoing search for the molecular basis of plant osmosensing. J. Gen. Physiol. *145*, 389–394.

Heo, J., Meng, F., and Hua, S.Z. (2008). Contribution of aquaporins to cellular water transport observed by a microfluidic cell volume sensor. Anal. Chem. *80*, 6974–6980.

Hohmann, S. (2009). Control of high osmolarity signalling in the yeast Saccharomyces cerevisiae. FEBS Lett. *583*, 4025–4029.

Holehouse, A.S., and Sukenik, S. (2020). Controlling Structural Bias in Intrinsically Disordered Proteins Using Solution Space Scanning. J. Chem. Theory Comput. *16*, 1794–1805.

Hosseiniyan Khatibi, S.M., Zununi Vahed, F., Sharifi, S., Ardalan, M., Mohajel Shoja, M., and Zununi Vahed, S. (2019). Osmolytes resist against harsh osmolarity: Something old something new. Biochimie *158*, 156–164.

Jalihal, A.P., Pitchiaya, S., Xiao, L., Bawa, P., Jiang, X., Bedi, K., Parolia, A., Cieslik, M., Ljungman, M., Chinnaiyan, A.M., et al. (2020). Multivalent Proteins Rapidly and Reversibly Phase-Separate upon Osmotic Cell Volume Change. Mol. Cell *79*, 978–990.e5.

Jones, A.M., Danielson, J.A., Manojkumar, S.N., Lanquar, V., Grossmann, G., and Frommer, W.B. (2014). Abscisic acid dynamics in roots detected with genetically encoded FRET sensors. Elife *3*, e01741.

Kaper, T., Lager, I., Looger, L.L., Chermak, D., and Frommer, W.B. (2008). Fluorescence resonance energy transfer sensors for quantitative monitoring of pentose and disaccharide accumulation in bacteria. Biotechnol. Biofuels *1*, 11.

Keul, N.D., Oruganty, K., Schaper Bergman, E.T., Beattie, N.R., McDonald, W.E., Kadirvelraj, R., Gross, M.L., Phillips, R.S., Harvey, S.C., and Wood, Z.A. (2018). The entropic force generated by intrinsically disordered segments tunes protein function. Nature *563*, 584–588.

Klipp, E., Nordlander, B., Krüger, R., Gennemark, P., and Hohmann, S. (2005). Integrative model of the response of yeast to osmotic shock. Nat. Biotechnol. *23*, 975–982.

Kroschwald, S., Maharana, S., and Simon, A. (2017). Hexanediol: a chemical probe to investigate the material properties of membrane-less compartments. Matters.

Li, X. (2011). Infiltration of Nicotiana benthamiana Protocol for Transient Expression via Agrobacterium. Bio Protoc. *1*.

Li, Y., Konstantopoulos, K., Zhao, R., Mori, Y., and Sun, S.X. (2020). The importance of water and hydraulic pressure in cell dynamics. J. Cell Sci. *133*.

Liu, B., Poolman, B., and Boersma, A.J. (2017). Ionic Strength Sensing in Living Cells. ACS Chem. Biol. *12*, 2510–2514.

Maeda, T., Takekawa, M., and Saito, H. (1995). Activation of yeast PBS2 MAPKK by MAPKKKs or by binding of an SH3-containing osmosensor. Science *269*, 554–558.

Mahon, M.J. (2011). pHluorin2: an enhanced, ratiometric, pH-sensitive green florescent protein. Adv. Biosci. Biotechnol. *2*, 132–137.

McGibbon, R.T., Beauchamp, K.A., Harrigan, M.P., Klein, C., Swails, J.M., Hernández, C.X., Schwantes, C.R., Wang, L.-P., Lane, T.J., and Pande, V.S. (2015). MDTraj: A Modern Open Library for the Analysis of Molecular Dynamics Trajectories. Biophys. J. *109*, 1528–1532.

Mergner, J., Frejno, M., List, M., Papacek, M., Chen, X., Chaudhary, A., Samaras, P., Richter, S., Shikata, H., Messerer, M., et al. (2020). Mass-spectrometry-based draft of the Arabidopsis proteome. Nature *579*, 409–414.

Mika, J.T., and Poolman, B. (2011). Macromolecule diffusion and confinement in prokaryotic cells. Curr. Opin. Biotechnol. *22*, 117–126.

Mittal, A., Das, R., Vitalis, A., and Pappu, R. (2014). ABSINTH Implicit Solvation Model and Force Field Paradigm for Use in

Simulations of Intrinsically Disordered Proteins. Computational Approaches to Protein Dynamics: From Quantum to Coarse-Grained Methods 181.

Moses, D., Yu, F., Ginell, G.M., Shamoon, N.M., Koenig, P.S., Holehouse, A.S., and Sukenik, S. (2020). Revealing the Hidden Sensitivity of Intrinsically Disordered Proteins to their Chemical Environment. J. Phys. Chem. Lett. *11*, 10131–10136.

Nongpiur, R.C., Singla-Pareek, S.L., and Pareek, A. (2020). The quest for osmosensors in plants. J. Exp. Bot. *71*, 595–607.

Okumoto, S., Jones, A., and Frommer, W.B. (2012). Quantitative imaging with fluorescent biosensors. Annu. Rev. Plant Biol. *63*, 663–706.

Olvera-Carrillo, Y., Campos, F., Reyes, J.L., Garciarrubio, A., and Covarrubias, A.A. (2010). Functional analysis of the group 4 late embryogenesis abundant proteins reveals their relevance in the adaptive response during water deficit in Arabidopsis. Plant Physiol. *154*, 373–390.

Persson, L.B., Ambati, V.S., and Brandman, O. (2020). Cellular Control of Viscosity Counters Changes in Temperature and Energy Availability. Cell *0*.

Pittas, T., Zuo, W., and Boersma, A.J. (2020). Engineering crowding sensitivity into protein linkers. In Methods in Enzymology, (Academic Press),.

Ranjit, S., Malacrida, L., Jameson, D.M., and Gratton, E. (2018). Fit-free analysis of fluorescence lifetime imaging data using the phasor approach. Nat. Protoc. *13*, 1979–2004.

Record, M.T., Jr, Courtenay, E.S., Cayley, D.S., and Guttman, H.J. (1998). Responses of E. coli to osmotic stress: large changes in amounts of cytoplasmic solutes and water. Trends Biochem. Sci. *23*, 143–148.

Rep, M., Krantz, M., Thevelein, J.M., and Hohmann, S. (2000). The transcriptional response of Saccharomyces cerevisiae to osmotic shock. Hot1p and Msn2p/Msn4p are required for the induction of subsets of high osmolarity glycerol pathway-dependent genes. J. Biol. Chem. *275*, 8290–8300.

Scharwies, J.D., and Dinneny, J.R. (2019). Water transport, perception, and response in plants. J. Plant Res. *132*, 311–324.

Shin, Y., and Brangwynne, C.P. (2017). Liquid phase condensation in cell physiology and disease. Science *357*.

Spitzer, J., and Poolman, B. (2009). The role of biomacromolecular crowding, ionic strength, and physicochemical gradients in the complexities of life's emergence. Microbiol. Mol. Biol. Rev. *73*, 371–388.

Sukenik, S., Ren, P., and Gruebele, M. (2017). Weak protein–protein interactions in live cells are quantified by cell-volume modulation. Proc. Natl. Acad. Sci. U. S. A. *114*, 6776–6781.

Theillet, F.-X., Binolfi, A., Frembgen-Kesner, T., Hingorani, K., Sarkar, M., Kyne, C., Li, C., Crowley, P.B., Gierasch, L., Pielak, G.J., et al. (2014). Physicochemical properties of cells and their effects on intrinsically disordered proteins (IDPs). Chem. Rev. *114*, 6661–6714.

Tompa, P. (2005). The interplay between structure and function in intrinsically unstructured proteins. FEBS Lett. *579*, 3346–3354.

Uversky, V.N., Oldfield, C.J., and Dunker, A.K. (2008). Intrinsically disordered proteins in human diseases: introducing the D2 concept. Annu. Rev. Biophys. *37*, 215–246.

Van Roey, K., Uyar, B., Weatheritt, R.J., Dinkel, H., Seiler, M., Budd, A., Gibson, T.J., and Davey, N.E. (2014). Short linear motifs: ubiquitous and functionally diverse protein interaction modules directing cell regulation. Chem. Rev. *114*, 6733–6778.

Vitalis, A., and Pappu, R.V. (2009). ABSINTH: a new continuum solvation model for simulations of polypeptides in aqueous solutions. J. Comput. Chem. *30*, 673–699.

Wright, P.E., and Dyson, H.J. (2015). Intrinsically disordered proteins in cellular signalling and regulation. Nat. Rev. Mol. Cell Biol. *16*, 18–29.

Yancey, P.H. (2005). Organic osmolytes as compatible, metabolic and counteracting cytoprotectants in high osmolarity and other stresses. J. Exp. Biol. *208*, 2819–2830.

Yoo, H., Triandafillou, C., and Drummond, D.A. (2019). Cellular sensing by phase separation: Using the process, not just the products. J. Biol. Chem. *294*, 7151–7159.

Zhang, X., Henriques, R., Lin, S.-S., Niu, Q.-W., and Chua, N.-H. (2006). Agrobacterium-mediated transformation of Arabidopsis thaliana using the floral dip method. Nat. Protoc. *1*, 641–646.

Zhou, X., Mehta, S., and Zhang, J. (2020). Genetically Encodable Fluorescent and Bioluminescent Biosensors Light Up Signaling Networks. Trends Biochem. Sci. *45*, 889–905.